ACS APPLIED MATERIALS & INTERFACES

www.acsami.org

Research Article

Aliovalent Doping of CeO_2 Improves the Stability of Atomically Dispersed Pt

Haodong Wang, Matthew Kottwitz, Ning Rui, Sanjaya D. Senanayake, Nebojsa Marinkovic, Yuanyuan Li,* Ralph G. Nuzzo,* and Anatoly I. Frenkel*

Cite This: *ACS Appl. Mater. Interfaces* 2021, 13, 52736–52742

Read Online

ACCESS | Metrics & More | Article Recommendations | Supporting Information

ABSTRACT: Atomically dispersed supported catalysts hold considerable promise as catalytic materials. The ability to employ and stabilize them against aggregation in complex process environments remains a key challenge to the elusive goal of 100% atom utilization in catalysis. Herein, using a Gd-doped ceria support for atomically dispersed surface Pt atoms, we establish how the combined effects of aliovalent doping and oxygen vacancy generation provide dynamic mechanisms that serve to enhance the stability of supported single-atom configurations. Using correlated, in situ X-ray absorption, photoelectron, and vibrational spectroscopy methods for the analysis of samples on the two types of support (with and without Gd doping), we establish that the Pt atoms are located proximal to Gd dopants, forming a speciation that serves to enhance the thermal stability of Pt atoms against aggregation.

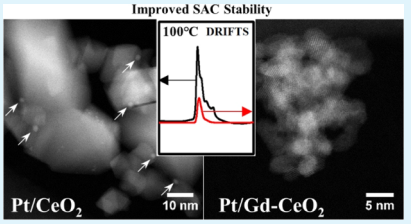

KEYWORDS: *aliovalent doping, catalysis, metal-support, single atom, vacancies*

INTRODUCTION

The stability of working atomically dispersed noble-metal catalysts, often termed "single-atom catalysts" (SACs), is one of the key factors that affects their efficiency and potential applications in industry. To improve the stability of SACs, one strategy is to stabilize single atoms on reducible supports via surface defects such as oxygen vacancies.[1−5] In addition to this, active oxygen vacancies on reducible metal oxides are considered to be essential for many redox reactions.[6] Reducible oxide supports, particularly CeO_2, have been used and researched extensively in the area of heterogeneous catalysis due to their ability to support atomically dispersed metal species and increase the mobility of oxygen atoms necessary for some catalytic pathways.[3,5,7−9] These capabilities of ceria can be enhanced by aliovalent doping, specifically, using dopants with valence lower than Ce(IV), thereby creating oxygen vacancies and improving oxygen activation.[6] For example, in Gd(III)-doped ceria in the doping range of 20 to 50%, it was reported that Gd−vacancy complexes were formed.[10,11] On the other hand, the inclusion of dopants affects the physical properties of the ceria support which in turn leads to the modification of the single metal−support interaction, the electronic structure and geometry of active single-atom sites, and their catalytic behavior under realistic conditions.[12−14] Thus, aliovalent doping is an attractive strategy for stabilizing single-atom catalysts, but there are no studies, to the best of our knowledge, focusing on the atomic-level details of the catalyst−support interaction, required for understanding their enhanced stability.

We hypothesize that the effect of a substitutional dopant M(III) into the CeO_2 structure will modify not only the bulk but also the surface of CeO_2 and create new types of sites for anchoring single atoms, as shown schematically in Figure 1.

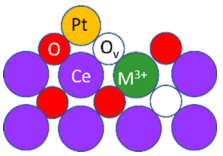

Figure 1. Simplified cartoon of the proposed Pt single-atom sites introduced by aliovalently doped ceria. The dopant, M(III), is shown by a green circle. The host, Ce(IV), is shown by purple circles.

Thus, for systematically investigating the role of doped support in SAC stability, it is required to both detect the presence of vacancy in the local environment of SACs and monitor the changes in the chemical state and structure of SACs at elevated temperatures and under reducing conditions.

In this work, as a demonstration of the aliovalent doping effect, we used Gd(III) as a substitutional dopant in CeO_2 and observed the enhanced thermal stability of isolated Pt species supported on doped CeO_2 compared to the undoped support. We hypothesize that the origin of such an improved stability of atomically dispersed catalysts supported on doped reducible

Received: September 22, 2021
Accepted: October 19, 2021
Published: October 29, 2021

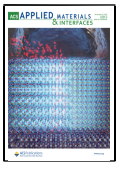

https://doi.org/10.1021/acsami.1c18330
ACS Appl. Mater. Interfaces 2021, 13, 52736−52742

oxides must be linked to the doping-induced changes in the catalytic active sites. This understanding is currently lacking, to the best of our knowledge.

At the limit of single metal atoms on the support, ensemble-averaging techniques such as X-ray absorption fine structure spectroscopy (XAFS) should be combined with complementary probes to validate the atomic dispersion, discriminate between different structures and electronic states of the coexisting metal species, and monitor their changes under similar environmental conditions. To that end, we performed ex situ scanning transmission electron microscopy (STEM), in situ diffuse reflectance infrared Fourier transform spectroscopy (DRIFTS), and ambient pressure X-ray photoelectron spectroscopy (AP-XPS). As a result of correlation between multiple experimental data, we found an explanation for the enhanced stability of Pt atoms on the Gd-doped support.

RESULTS AND DISCUSSION

Two samples were prepared via a standard wet impregnation method on either commercial CeO_2 or commercial 20 mol % Gd-doped CeO_2 (Gd−CeO_2). To prevent aggregation, we used a sufficiently low concentration of Pt atoms in solution. The details of the preparation are given in the Supporting Information. Table 1 provides a summary of the surface

Table 1. Summary of Pt Loadings

support	weight loading (wt % Pt)	surface area (m^2/g)	Pt surface loading (atoms/nm^2)
CeO_2	0.28	44.73	0.192
Gd−CeO_2	1.42	160.9	0.272

loadings (Pt atoms/area of support) for the two samples, as computed from the Pt weight loadings measured by inductively coupled plasma (ICP) spectrometry and support BET surface areas.

The structure of the supported Pt samples was examined by STEM (Figure 2). Lattice fringes attest to the crystalline nature of the CeO_2 and Gd−CeO_2 supports in Figure 2a,b, respectively. It was previously reported that the doping of rare-earth metals into CeO_2 causes changes in the specific surface area, particle size, and morphology of ceria.[15] To ensure that the two samples had similar Pt surface loadings after deposition (the higher the surface loading, the easier it is for the Pt atoms to aggregate[16]), different weight loadings were used to adjust for the difference in the surface area between the two samples (Figure 2a,b and Table 1). Neither Figure 2a,b nor the additional examples provided in Figure S1 (Supporting Information) provide any sign of aggregated or clustered Pt atoms on the surface of either support. Isolated bright spots suggestive of individual Pt atoms were observed in both as-prepared samples. Ex situ STEM micrographs of the samples following thermal treatment at 100 °C under a reducing CO atmosphere provide evidence of aggregation for the Pt/CeO_2 sample (Figure 2c) but not for the Pt/Gd−CeO_2 sample (Figure 2d). In situ CO-probe DRIFTS verified the uniformity of the distribution of single atoms on both supports. For understanding the distribution of charge states of Pt atoms, we performed in situ AP-XPS studies.

DRIFTS spectra for the Pt/CeO_2 and Pt/Gd−CeO_2 samples are shown in Figure 3a. The characteristic peaks that appear between 1800 and 2200 cm^{-1} correspond to the vibrational/stretching modes of CO adsorbed onto Pt sites.[17−19] At room

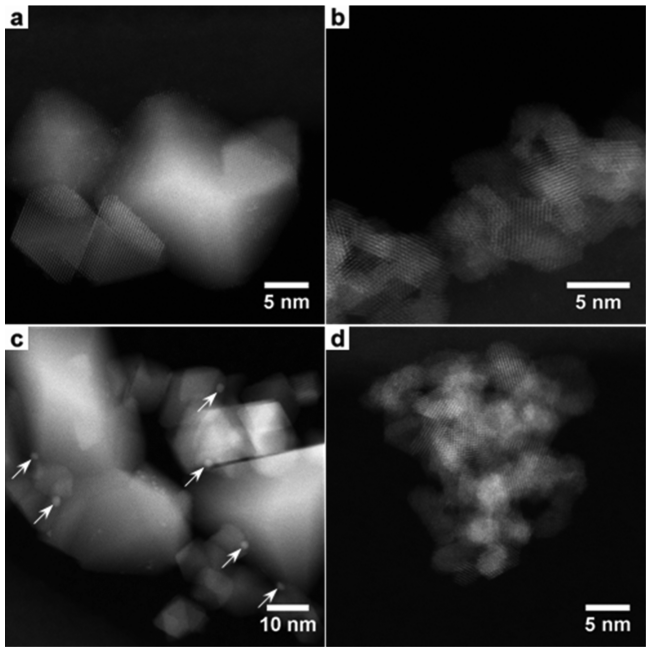

Figure 2. STEM images of the as-prepared Pt/CeO_2 (a) and Pt/Gd−CeO_2 (b) samples lack evidence of Pt aggregation. After treatment with CO at 100 °C, noticeable aggregation is observed (as indicated by arrows) for the Pt/CeO_2 sample (c) but not for the Pt/Gd−CeO_2 sample (d).

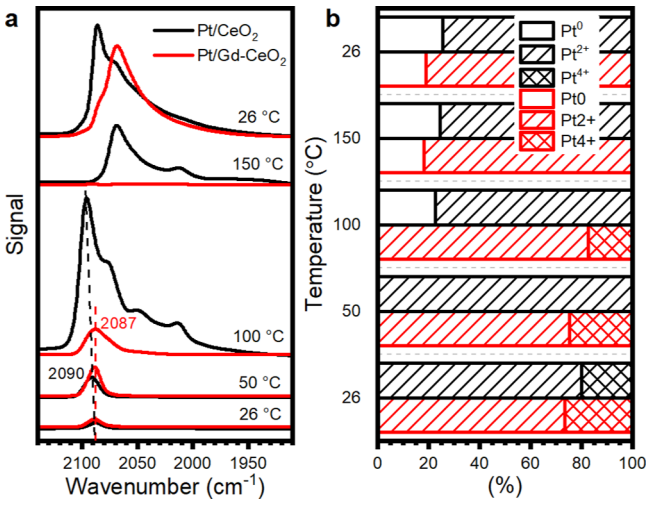

Figure 3. (a) CO-probed DRIFTS spectra of the Pt/CeO_2 (black) and Pt/Gd−CeO_2 (red) samples. Correspondingly, two dashed lines were used to indicate the shifts of the CO bands for these two samples. The data were collected after CO (20% balance in He) was flushed away by helium. (b) Distribution of Pt oxidation states observed under CO (20% balance in He) by AP-XPS of the Pt/CeO_2 (black) and Pt/Gd−CeO_2 (red) samples at in-situ temperatures (26−50−100−150−26 °C).

temperature, both samples display a single narrow peak at 2087 cm^{-1} assigned to CO linearly adsorbed onto isolated $Pt^{\delta+}$ species.[20] Thus, DRIFTS measurements independently confirm our preliminary conclusion from Figure 2a,b that Pt was atomically dispersed on the supports of the as-prepared samples. Furthermore, the in situ DRIFTS measurements (*vide infra*) illustrate the differences that exist in the electronic structure and geometry of Pt single atoms, perturbations that by direct inference must be caused by likely proximal

https://doi.org/10.1021/acsami.1c18330
ACS Appl. Mater. Interfaces 2021, 13, 52736−52742

interactions with the Gd dopant sites. First, at 50 °C, a single narrow peak is observed in both samples; while its position is observed at 2087 cm^{-1} for the Pt/Gd−CeO_2 sample, it is shifted to 2090 cm^{-1} for the Pt/CeO_2 sample. Such difference in the positions of the CO-bound peak on isolated $Pt^{\delta+}$ species (shown by arrows in Figure 3a) is also observed at 100 °C. Second, in addition to that, at 100 °C, other peaks are readily apparent for the Pt/CeO_2 sample, while the Pt/Gd−CeO_2 sample displays a subtle broadening. For the Pt/CeO_2 sample, those peaks between 2075 and 2010 cm^{-1} are assigned to CO linearly adsorbed onto generally more reduced or clustered Pt species than the peak at 2087 cm^{-1}.[21] Besides, the increased intensity of Pt/CeO_2 spectra can also be related to the partial reduction of Pt species.[22] These spectra at 100 °C confirm the clustering observed for the Pt/CeO_2 sample (Figure 2c), as well as the lack of clustering observed for the Pt/Gd−CeO_2 sample (Figure 2d). Third, we note that the spectral features at 150 °C are notably weaker in the case of Pt/CeO_2 or absent in the case of Pt/Gd−CeO_2 due to a reduced population of bound CO states arising from the higher thermal energy present in the system and suggests a weak binding strength for CO adsorbed onto the Pt species, especially in the Pt/Gd−CeO_2 sample. After subsequent cooling to 26 °C, pronounced peaks were observed in both samples. The reason that the two spectra are different could be due to the formation of Pt clusters/particles with different sizes.[23] Overall, between the two samples, these differences in the position, intensity, and changing trend of bound CO peaks detailed above are attributed to the perturbation of the electronic structure and geometry of Pt single-atom species caused by the Gd dopants. Quantitative assignments of the formal oxidation states of Pt in each system and an independent verification of the conclusions drawn on the basis of STEM and DRIFTS measurements were made by the AP-XPS studies at the same temperatures.

Figure 3b shows the fitting results of Pt 4f XPS core-level data for the Pt/CeO_2 and Pt/Gd−CeO_2 samples. The raw spectra and peak-fitting results for each sample at each temperature are given in Figure S2 (Supporting Information). At room temperature, both samples are dominated by Pt^{2+} species with the coexistence of a small fraction of Pt^{4+} species (20% in Pt/CeO_2 and 27% in Pt/Gd−CeO_2). All the Pt^{4+} species are reduced to Pt^{2+} for the Pt/CeO_2 sample at 50 °C, while only 2% (out of 27% Pt^{4+}) are reduced to Pt^{2+} at the same temperature for the Pt/Gd−CeO_2 sample, suggesting the different nature of Pt^{4+} species in the two samples. At 100 °C, peaks assigned to Pt^0 (23%) appear only in the spectra of the Pt/CeO_2 sample, suggesting the formation of metallic Pt species, in agreement with the results obtained via CO-probed DRIFTS at the same temperature. The formation of Pt metallic species is not observed until 150 °C for the Pt/Gd−CeO_2 sample, suggesting that in the Pt/Gd−CeO_2 sample, the Pt single-atom species are more resistant to aggregation, which could be due to the modified metal−support interaction by Gd dopants. To get more insights into the effects of metal−support interaction on the electronic and atomic structure of Pt single-atom species, XAFS measurements were performed.

The Pt L_3-edge X-ray absorption near-edge structure (XANES) spectra (Figure 4a) reveal the changes in the electronic structure of the Pt species in the two samples during heating under the CO atmosphere. The white line peak in Pt L_3 XANES is a strong absorption maximum due to a 2p → 5d transition, and its area can be used as a measure of the density of unoccupied 5d states.[24,25] A comparison of the room-

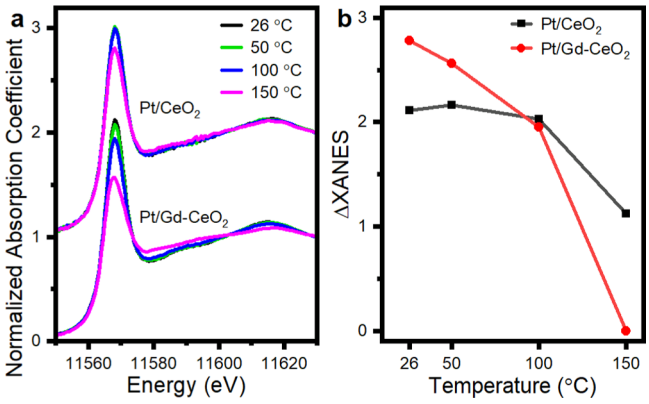

Figure 4. (a) In situ Pt L_3 edge XANES spectra of the Pt/CeO_2 and Pt/Gd−CeO_2 samples under a CO atmosphere (5% balance in He) at different temperatures and (b) the integrated intensity of the area of XANES difference spectra for each sample at each temperature compared to that of the Pt/Gd−CeO_2 sample at 150 °C. The energy range for calculating the area is from 11559 to 11573 eV.

temperature spectra of the Pt foil, α-PtO_2, Pt/CeO_2, and Pt/Gd−CeO_2 is shown in Supporting Information Figure S3. The white line intensity of Pt/Gd−CeO_2 is similar to that in the α-PtO_2 spectrum and higher than that in the spectrum of the Pt/CeO_2 sample. In the post-edge region, the deviation of the catalysts' data from that of PtO_2 clearly indicates the unique structure of the catalysts. The integrated area of the difference in the XANES region for Pt/CeO_2 and Pt/Gd−CeO_2 at each temperature is shown in Figure 4b, with the spectra of the Pt/Gd−CeO_2 sample at 150 °C used as the reference for all the spectra. The Pt/CeO_2 sample spectra show almost no intensity changes in the white line region upon heating from room temperature to 100 °C and a relatively small change upon heating to 150 °C, as compared to the Pt/Gd−CeO_2 sample. The decrease of the white line peak intensity is more significant in the Pt/Gd−CeO_2 sample. The greater change in the white line of the Pt/Gd−CeO_2 sample indicates that the average electronic density of the Pt species changes more rapidly than that of the Pt/CeO_2 sample: in the Gd-doped sample, Pt atoms easily gain electrons in d-states by increasing the temperature under CO.[26,27] The greater change in the white line of the Pt/Gd−CeO_2 sample cannot be solely explained by the temperature-dependent changes in the speciation, as observed by AP-XPS (Figure 3b), which indicates that the Pt species are more easily reduced in the Pt/CeO_2 sample, in seeming contradiction with the trends shown in Figure 4. To reveal the factors that affect the d states of Pt species, we performed extended X-ray absorption fine structure (EXAFS) analysis to provide information about the local coordination environment of Pt species.

The Fourier transform magnitudes of the EXAFS data for the two samples under the same treatment as in the DRIFTS and AP-XPS measurements are shown in Figure 5a. For both samples, there is a pronounced peak at about 1.6 Å, corresponding to the first shell Pt−O contribution. Generally, with the increase of the temperature, the intensity of Pt−O peak decreases. For the peaks in the higher R range (2.0−3.5 Å), multiple photoelectron scattering paths were examined and considered for including in the fitting model (the details are provided in Supporting Information Table S1). Except for the spectrum of the Pt/CeO_2 collected at 150 °C, the best model consists of a Pt−O bond at approximately 2.0 Å, a Pt−Ce

https://doi.org/10.1021/acsami.1c18330
ACS Appl. Mater. Interfaces 2021, 13, 52736−52742

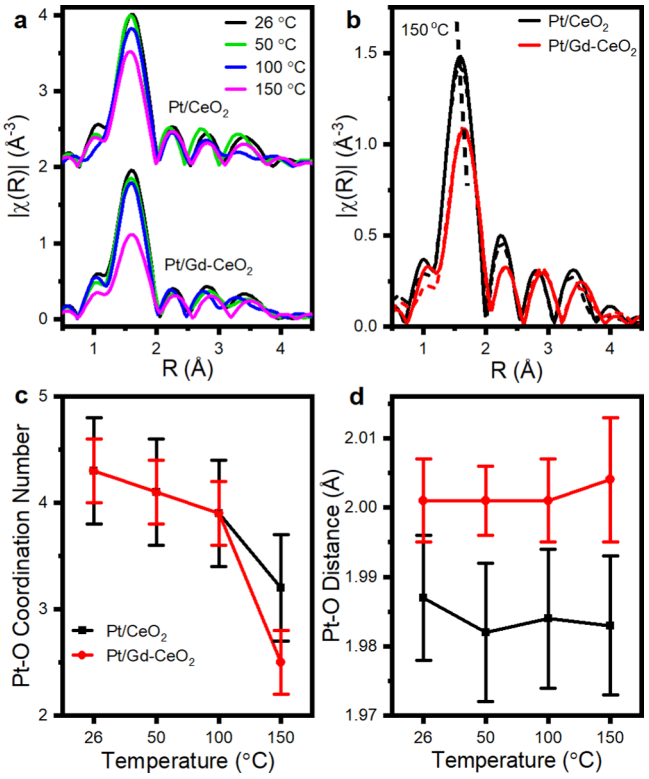

Figure 5. (a) Temperature-dependent Fourier transform magnitudes of k^2-weighted EXAFS spectra of the Pt/CeO_2 and $Pt/Gd-CeO_2$ samples under a CO atmosphere at different temperatures. All data were collected at room temperature after high-temperature treatment. (b) Comparison of experimental spectra with the fit (dash line) for Pt/CeO_2 and $Pt/Gd-CeO_2$ samples under a CO atmosphere at room temperature after 150 °C treatment. The first shell Pt−O coordination numbers (c) and interatomic distances (d), as determined from the fitting of EXAFS spectra for Pt/CeO_2 (black) and $Pt/Gd-CeO_2$ (red).

contribution at 3.2 Å, a Pt−O contribution at 3.6 Å, and a Pt−Ce contribution at 3.9 Å. This model is consistent with the optimized Pt single-atom structures proposed by DFT calculations.[28,29] For the spectrum of Pt/CeO_2 collected at 150 °C, the Pt−Pt scattering path corresponding to a metallic bond was required to achieve a good fit, suggesting, again, that the Pt species in the $Pt/Gd-CeO_2$ sample are more resistant to clustering than in the Pt/CeO_2 sample. As a result of the use of different in situ reactors for DRIFTS, AP-XPS and XAFS, the aggregation of Pt single atoms for the Pt/CeO_2 sample occurred at approximately 100 °C in DRIFTS and AP-XPS experiments, whereas it was first observed at 150 °C in XAFS measurements. We will thus correlate the results obtained from different techniques based on the temperature-dependent changes instead of actual temperatures. Quantitative fitting results of EXAFS data are summarized in Supporting Information Table S2. The data and the fits for all samples and temperatures are shown in Supporting Information Figure S4. Out of several DFT-optimized structural models of the Pt environment with four Pt−O nearest neighbor bonds,[28] the model (denoted as D4 in ref 28) in which Pt atoms had short (3.3 Å) and long (3.9−4.2 Å) Pt−Ce distances proved to be the best for describing the experimental data for both supports. We note that EXAFS analysis does not distinguish between Ce or Gd as a backscattering atom,[30] due to their proximity in the periodic table. We hypothesize that the Pt−Ce coordination reported for both the supports (Supporting Information Table S2) represents both Pt−Ce and Pt−Gd pairs for the $Gd-CeO_2$ support, as explained in greater detail below.

We now focus on what is learned from the trends in coordination numbers and interatomic distances. As shown in Figure 5c, at 26, 50, and 100 °C, the coordination numbers of the nearest Pt−O bond are nearly the same (the mean values vary between 4.3 and 3.9) for both samples. Further increasing the temperature results in an abrupt decrease of the Pt−O coordination number. For the Pt/CeO_2 sample, from 100 to 150 °C, the coordination number of Pt−O drops by ca. 18% (from 3.9 to 3.2), and for the $Pt/Gd-CeO_2$ sample, it is reduced by 36% (from 3.9 to 2.5). When combined with AP-XPS results, the explanation for the slow decrease of the Pt−O coordination number from 26 to 100 °C is mostly likely due to the reduction of a small fraction of Pt^{4+} to the dominating Pt^{2+} single-atom species. For the Pt/CeO_2 sample, at 150 °C, the sudden drop in the Pt−O coordination number is due to the formation of Pt metallic clusters, evidenced also by the emerging of the Pt−Pt bond in EXAFS at that temperature. According to the Pt−O coordination numbers, about 20% $[\Delta N/N = (4 - 3.2)/4 = 0.2]$ Pt atoms aggregate into clusters, that is, very similar to the fraction of 23%, the concentration of Pt^0 obtained from AP-XPS. Interestingly, for the $Pt/Gd-CeO_2$ sample, the greater drop in the first neighboring O atoms does not result in the formation of Pt clusters, which were not detected at 150 °C. These results suggest that even though at low temperatures (26, 50, and 100 °C), the coordination number of Pt−O is similar for both samples, the electronic structure and the geometry of Pt single-atom species are different, thus causing different temperature-dependent changes observed in DRIFTS (Figure 3a), AP-XPS (Figure 3b), XANES (Figure 4), and EXAFS (Figure 5d). It was previously reported that the catalytic properties of single-atom catalysts correlated with the number of neighboring atoms around single atoms.[29,31,32] Our combined results reveal that the coordination number (same for the as-prepared samples, but the Gd-doped support showed improved stability for Pt single-atom species) is not the only descriptor determining the catalytic stability of single-atom catalysts.

The Pt−O interatomic distances (Figure 5b,d) so determined are consistently longer for the $Pt/Gd-CeO_2$ sample compared to those found for the Pt/CeO_2 material. As shown by Kossoy et al., a solid solution of 20 at % Gd in CeO_2 features structural buckling of the lattice, whereas Gd−O distances are distinctly longer than the host Ce−O distances.[33] Similar results were obtained by EXAFS in other binary solid solutions $A_yB_{1-y}X$, in which the larger cation A had a longer distance to a common anion X as compared to a smaller cation B.[34−38] Hence, we propose that the longer first shell Pt−O distances in the $Pt/Gd-CeO_2$ sample provide evidence that a significant fraction of Pt species is proximal to surface Gd sites. The existence of these Gd dopants modifies the electronic structure and geometry of the Pt single atoms anchored on the ceria support as discussed above. In addition to it, the Gd dopants improve the reducibility of ceria: at 150 °C, for each Pt single atom, on average, the ceria support offers from 3.2 to 4 nearest neighbor oxygen atoms in Pt/CeO_2 but only 2.5 in the $Pt/Gd-CeO_2$. Correspondingly, Gd introduces 0.7−1.5 more oxygen vacancies near the Pt single atoms. The combined effect of proximal Gd(III) and oxygen vacancies modifies the electronic structure and geometry of Pt single atoms, and, together with the increased number of oxygen

https://doi.org/10.1021/acsami.1c18330
ACS Appl. Mater. Interfaces 2021, 13, 52736−52742

vacancies in the ceria support, strengthen the metal−support interaction. The latter conclusion is supported by the evidence of enhanced charge transfer between Pt single atoms and the support (Figure 4b) and, in turn, provides the explanation for the enhanced stability of Pt single atoms on aliovalently doped support.

Combining the information from all experimental data, different scenarios of the evolution of atomically dispersed Pt species under a CO atmosphere that were studied for the two types of support, pure ceria and Gd-doped ceria, are shown schematically in Figure 6.

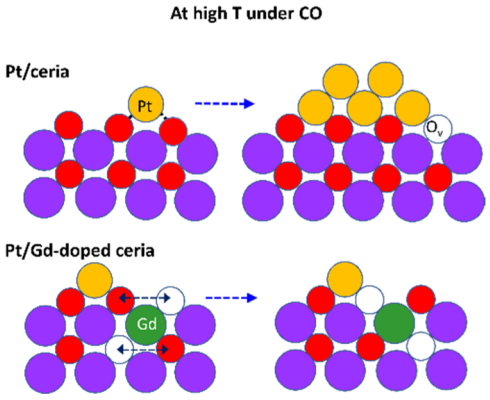

Figure 6. Simplified cartoon of the evolution of Pt species and sites in the Pt/ceria and Pt/Gd-doped ceria samples under a CO atmosphere at elevated temperatures. For the Pt/ceria sample, the breaking of the Pt−O bond results in the aggregation of Pt atoms. For the Pt/Gd-doped ceria sample, the increased concentration of oxygen vacancies and the mobility of oxygen atoms (dashed black arrows) caused by the Gd doping lead to stable Pt−oxygen vacancy (O_v)−Ce/Gd sites.

CONCLUSIONS

In summary, we have shown that, on the Gd-doped CeO_2 support, Pt atoms prefer to be located at the four-coordinated sites proximal to surface-localized Gd atoms. The inclusion of Gd as a dopant in a CeO_2 support modifies the electronic structures and geometries of the Pt single-atom species and increases the number of oxygen vacancies neighbored to Pt single atoms, resulting in the enhanced metal−support interaction and the stability of Pt single atoms. Tuning the metal−support interaction by a combined effect of aliovalent doping and oxygen vacancies provides a new pathway for improved stability and reducibility of the ceria support. We propose that these properties will also open new opportunities for modifying the activity of Pt single-atom sites in redox reactions.

ASSOCIATED CONTENT

Supporting Information

The Supporting Information is available free of charge at https://pubs.acs.org/doi/10.1021/acsami.1c18330.

Experimental details and additional characterization data including STEM images, DRIFTS spectra, XPS spectra, and XAS spectra (PDF)

AUTHOR INFORMATION

Corresponding Authors

Yuanyuan Li − *Department of Materials Science and Chemical Engineering, Stony Brook University, Stony Brook, New York 11794, United States;* orcid.org/0000-0003-3074-9672; Email: yyli@bnl.gov

Ralph G. Nuzzo − *Department of Chemistry, University of Illinois, Urbana, Illinois 61801, United States; Surface and Corrosion Science, School of Engineering Sciences in Chemistry, Biotechnology and Health, KTH Royal Institute of Technology, Stockholm 10044, Sweden*; Email: r-nuzzo@illlinois.edu

Anatoly I. Frenkel − *Department of Materials Science and Chemical Engineering, Stony Brook University, Stony Brook, New York 11794, United States; Chemistry Division, Brookhaven National Laboratory, Upton, New York 11973, United States;* orcid.org/0000-0002-5451-1207; Email: anatoly.frenkel@stonybrook.edu

Authors

Haodong Wang − *Department of Materials Science and Chemical Engineering, Stony Brook University, Stony Brook, New York 11794, United States;* orcid.org/0000-0002-2344-2456

Matthew Kottwitz − *Department of Chemistry, University of Illinois, Urbana, Illinois 61801, United States*

Ning Rui − *Chemistry Division, Brookhaven National Laboratory, Upton, New York 11973, United States;* orcid.org/0000-0001-6234-7075

Sanjaya D. Senanayake − *Chemistry Division, Brookhaven National Laboratory, Upton, New York 11973, United States;* orcid.org/0000-0003-3991-4232

Nebojsa Marinkovic − *Department of Chemical Engineering, Columbia University, New York, New York 10027, United States*

Complete contact information is available at: https://pubs.acs.org/10.1021/acsami.1c18330

Notes

The authors declare no competing financial interest.

ACKNOWLEDGMENTS

A.I.F. and R.G.N. acknowledge support of the U.S. DOE BES grant no. DE-SC0022199. DRIFTS measurements at Brookhaven National Laboratory were made possible due to the Program Development fund 21-017 to A.I.F. Work by S.D.S. and N.R. at Brookhaven National Laboratory was supported by the U.S. DOE BES under contract no. DE-SC0012704. S.D.S. was partially supported by a U.S. DOE Early Career Award. M.K. acknowledges the fellowship support from the Department of Chemistry at the University of Illinois. This research used beamline 7-BM (QAS) of the National Synchrotron Light Source II, a U.S. DOE Office of Science User Facility operated for the DOE Office of Science by Brookhaven National Laboratory under contract no. DE-SC0012704. Beamline operations were supported in part by the Synchrotron Catalysis Consortium (U.S. DOE, Office of Basic Energy Sciences, grant no. DE-SC0012335). We thank Drs. S. Ehrlich and L. Ma for help with the beamline measurements at the QAS beamline. We are grateful to Dr. I. Lubomirsky for discussion of properties of Gd-doped CeO_2 and to Drs. A.

https://doi.org/10.1021/acsami.1c18330
ACS Appl. Mater. Interfaces 2021, 13, 52736−52742

Bruix and K. Neyman for discussion of theoretical models of Pt on the CeO_2 support.

REFERENCES

(1) Qiao, B.; Wang, A.; Yang, X.; Allard, L. F.; Jiang, Z.; Cui, Y.; Liu, J.; Li, J.; Zhang, T. Single-Atom Catalysis of CO Oxidation Using Pt1/FeOx. *Nat. Chem.* **2011**, *3*, 634−641.

(2) Duarte, R. B.; Krumeich, F.; van Bokhoven, J. A. Structure, Activity, and Stability of Atomically Dispersed Rh in Methane Steam Reforming. *ACS Catal.* **2014**, *4*, 1279−1286.

(3) Wan, J.; Chen, W.; Jia, C.; Zheng, L.; Dong, J.; Zheng, X.; Wang, Y.; Yan, W.; Chen, C.; Peng, Q.; Wang, D.; Li, Y. Defect Effects on TiO_2 Nanosheets: Stabilizing Single Atomic Site Au and Promoting Catalytic Properties. *Adv. Mater.* **2018**, *30*, 1705369.

(4) Wang, J.; Zhao, X.; Lei, N.; Li, L.; Zhang, L.; Xu, S.; Miao, S.; Pan, X.; Wang, A.; Zhang, T. Hydrogenolysis of Glycerol to 1,3-Propanediol under Low Hydrogen Pressure over WOx-Supported Single/Pseudo-Single Atom Pt Catalyst. *ChemSusChem* **2016**, *9*, 784−790.

(5) Nie, L.; Mei, D.; Xiong, H.; Peng, B.; Ren, Z.; Hernandez, X. I. P.; DeLaRiva, A.; Wang, M.; Engelhard, M. H.; Kovarik, L.; Datye, A. K.; Wang, Y. Activation of Surface Lattice Oxygen in Single-Atom Pt/CeO_2 for Low-Temperature CO Oxidation. *Science* **2017**, *358*, 1419−1423.

(6) Yu, K.; Lou, L.-L.; Liu, S.; Zhou, W. Asymmetric Oxygen Vacancies: The Intrinsic Redox Active Sites in Metal Oxide Catalysts. *Adv. Sci.* **2020**, *7*, 1901970.

(7) Jiang, D.; Wan, G.; García-Vargas, C. E.; Li, L.; Pereira-Hernández, X. I.; Wang, C.; Wang, Y. Elucidation of the Active Sites in Single-Atom Pd-1/CeO_2 Catalysts for Low-Temperature CO Oxidation. *ACS Catal.* **2020**, *10*, 11356−11364.

(8) Jan, A.; Shin, J.; Ahn, J.; Yang, S.; Yoon, K. J.; Son, J.-W.; Kim, H.; Lee, J.-H.; Ji, H.-I. Promotion of Pt/CeO_2 Catalyst by Hydrogen Treatment for Low-Temperature CO Oxidation. *RSC Adv.* **2019**, *9*, 27002−27012.

(9) Li, Y.; Kottwitz, M.; Vincent, J. L.; Enright, M. J.; Liu, Z.; Zhang, L.; Huang, J.; Senanayake, S. D.; Yang, W.-C. D.; Crozier, P. A.; Nuzzo, R. G.; Frenkel, A. I. Dynamic Structure of Active Sites in Ceria-Supported Pt Catalysts for the Water Gas Shift Reaction. *Nat. Commun.* **2021**, *12*, 941.

(10) Aparicio-Anglès, X.; Roldan, A.; de Leeuw, N. H. Gadolinium-Vacancy Clusters in the (111) Surface of Gadolinium-Doped Ceria: A Density Functional Theory Study. *Chem. Mater.* **2015**, *27*, 7910−7917.

(11) Coduri, M.; Checchia, S.; Longhi, M.; Ceresoli, D.; Scavini, M. Rare Earth Doped Ceria: The Complex Connection between Structure and Properties. *Front. Chem.* **2018**, *6*, 526.

(12) AlKhoori, A. A.; Polychronopoulou, K.; Belabbes, A.; Jaoude, M. A.; Vega, L. F.; Sebastian, V.; Hinder, S.; Baker, M. A.; Zedan, A. F. Cu, Sm Co-Doping Effect on the CO Oxidation Activity of CeO_2. A Combined Experimental and Density Functional Study. *Appl. Surf. Sci.* **2020**, *521*, 146305.

(13) Ricote, S.; Jacobs, G.; Milling, M.; Ji, Y.; Patterson, P. M.; Davis, B. H. Low Temperature Water-Gas Shift: Characterization and Testing of Binary Mixed Oxides of Ceria and Zirconia Promoted with Pt. *Appl. Catal., A* **2006**, *303*, 35−47.

(14) Vecchietti, J.; Bonivardi, A.; Xu, W.; Stacchiola, D.; Delgado, J. J.; Calatayud, M.; Collins, S. E. Understanding the Role of Oxygen Vacancies in the Water Gas Shift Reaction on Ceria-Supported Platinum Catalysts. *ACS Catal.* **2014**, *4*, 2088−2096.

(15) Dong, C.; Zong, X.; Jiang, W.; Niu, L.; Liu, Z.; Qu, D.; Wang, X.; Sun, Z. Recent Advances of Ceria-Based Materials in the Oxidation of Carbon Monoxide. *Small Struct.* **2021**, *2*, 2000081.

(16) Qin, R.; Liu, P.; Fu, G.; Zheng, N. Strategies for Stabilizing Atomically Dispersed Metal Catalysts. *Small Methods* **2018**, *2*, 1700286.

(17) Bazin, P.; Saur, O.; Lavalley, J. C.; Daturi, M.; Blanchard, G. FT-IR Study of CO Adsorption on Pt/CeO_2: Characterisation and Structural Rearrangement of Small Pt Particles. *Phys. Chem. Chem. Phys.* **2005**, *7*, 187−194.

(18) Happel, M.; Mysliveček, J.; Johánek, V.; Dvořák, F.; Stetsovych, O.; Lykhach, Y.; Matolín, V.; Libuda, J. Adsorption Sites, Metal-Support Interactions, and Oxygen Spillover Identified by Vibrational Spectroscopy of Adsorbed CO: A Model Study on Pt/Ceria Catalysts. *J. Catal.* **2012**, *289*, 118−126.

(19) Aleksandrov, H. A.; Neyman, K. M.; Hadjiivanov, K. I.; Vayssilov, G. N. Can the State of Platinum Species Be Unambiguously Determined by the Stretching Frequency of an Adsorbed CO Probe Molecule? *Phys. Chem. Chem. Phys.* **2016**, *18*, 22108−22121.

(20) Ding, K.; Gulec, A.; Johnson, A. M.; Schweitzer, N. M.; Stucky, G. D.; Marks, L. D.; Stair, P. C. Identification of Active Sites in CO Oxidation and Water-Gas Shift over Supported Pt Catalysts. *Science* **2015**, *350*, 189−192.

(21) Xie, P.; Pu, T.; Nie, A.; Hwang, S.; Purdy, S. C.; Yu, W.; Su, D.; Miller, J. T.; Wang, C. Nanoceria-Supported Single-Atom Platinum Catalysts for Direct Methane Conversion. *ACS Catal.* **2018**, *8*, 4044−4048.

(22) Daelman, N.; Capdevila-Cortada, M.; López, N. Dynamic Charge and Oxidation State of Pt/CeO_2 Single-Atom Catalysts. *Nat. Mater.* **2019**, *18*, 1215−1221.

(23) Lentz, C.; Jand, S. P.; Melke, J.; Roth, C.; Kaghazchi, P. DRIFTS Study of CO Adsorption on Pt Nanoparticles Supported by DFT Calculations. *J. Mol. Catal. A: Chem.* **2017**, *426*, 1−9.

(24) Mansour, A. N.; Cook, J. W.; Sayers, D. E. Quantitative Technique for the Determination of the Number of Unoccupied D-Electron States in a Platinum Catalyst Using the L2,3 X-Ray Absorption Edge Spectra. *J. Phys. Chem.* **1984**, *88*, 2330−2334.

(25) Brown, M.; Peierls, R. E.; Stern, E. A. White Lines in X-Ray Absorption. *Phys. Rev. B: Condens. Matter Mater. Phys.* **1977**, *15*, 738−744.

(26) Small, M. W.; Sanchez, S. I.; Marinkovic, N. S.; Frenkel, A. I.; Nuzzo, R. G. Influence of Adsorbates on the Electronic Structure, Bond Strain, and Thermal Properties of an Alumina-Supported Pt Catalyst. *ACS Nano* **2012**, *6*, 5583−5595.

(27) Timoshenko, J.; Wrasman, C. J.; Luneau, M.; Shirman, T.; Cargnello, M.; Bare, S. R.; Aizenberg, J.; Friend, C. M.; Frenkel, A. I. Probing Atomic Distributions in Mono- and Bimetallic Nanoparticles by Supervised Machine Learning. *Nano Lett.* **2019**, *19*, 520−529.

(28) Figueroba, A.; Bruix, A.; Kovács, G.; Neyman, K. M. Metal-Doped Ceria Nanoparticles: Stability and Redox Processes. *Phys. Chem. Chem. Phys.* **2017**, *19*, 21729−21738.

(29) Kottwitz, M.; Li, Y.; Palomino, R. M.; Liu, Z.; Wang, G.; Wu, Q.; Huang, J.; Timoshenko, J.; Senanayake, S. D.; Balasubramanian, M.; Lu, D.; Nuzzo, R. G.; Frenkel, A. I. Local Structure and Electronic State of Atomically Dispersed Pt Supported on Nanosized CeO_2. *ACS Catal.* **2019**, *9*, 8738−8748.

(30) Kossoy, A.; Frenkel, A. I.; Wang, Q.; Wachtel, E.; Lubomirsky, I. Local Structure and Strain-Induced Distortion in Ce0.8Gd0.2O1.9. *Adv. Mater.* **2010**, *22*, 1659−1662.

(31) Zhao, Q.; Liu, B.; Xu, Y.; Jiang, F.; Liu, X. Insight into the Active Site and Reaction Mechanism for Selective Oxidation of Methane to Methanol Using H_2O_2 on a Rh1/ZrO_2 Catalyst. *New J. Chem.* **2020**, *44*, 1632−1639.

(32) Pan, Y.; Chen, Y.; Wu, K.; Chen, Z.; Liu, S.; Cao, X.; Cheong, W.-C.; Meng, T.; Luo, J.; Zheng, L.; Liu, C.; Wang, D.; Peng, Q.; Li, J.; Chen, C. Regulating the Coordination Structure of Single-Atom Fe-NxCy Catalytic Sites for Benzene Oxidation. *Nat. Commun.* **2019**, *10*, 4290.

(33) Kossoy, A.; Wang, Q.; Korobko, R.; Grover, V.; Feldman, Y.; Wachtel, E.; Tyagi, A. K.; Frenkel, A. I.; Lubomirsky, I. Evolution of the Local Structure at the Phase Transition in CeO_2-Gd_2O_3 Solid Solutions. *Phys. Rev. B: Condens. Matter Mater. Phys.* **2013**, *87*, 054101.

(34) Frenkel, A.; Stern, E. A.; Voronel, A.; Qian, M.; Newville, M. Buckled Crystalline Structure of Mixed Ionic Salts. *Phys. Rev. Lett.* **1993**, *71*, 3485−3488.

https://doi.org/10.1021/acsami.1c18330
ACS Appl. Mater. Interfaces 2021, 13, 52736−52742

(35) Frenkel, A.; Stern, E. A.; Voronel, A.; Qian, M.; Newville, M. Solving the Structure of Disordered Mixed Salts. *Phys. Rev. B: Condens. Matter Mater. Phys.* **1994**, *49*, 11662−11674.
(36) Frenkel, A.; Voronel, A.; Katzir, A.; Newville, M.; Stern, E. A. Buckled Crystalline Structure of Disordered Mixed Salts. *Phys. Rev. B: Condens. Matter Mater. Phys.* **1995**, *208*−*209*, 334−336.
(37) Frenkel, A. I.; Stern, E. A.; Voronel, A.; Heald, S. M. Lattice Strains in Disordered Mixed Salts. *Solid State Commun.* **1996**, *99*, 67−71.
(38) Frenkel, A. I.; Pease, D. M.; Budnick, J. I.; Metcalf, P.; Stern, E. A.; Shanthakumar, P.; Huang, T. Strain-Induced Bond Buckling and Its Role in Insulating Properties of Cr-Doped V_2O_3. *Phys. Rev. Lett.* **2006**, *97*, 195502.

https://doi.org/10.1021/acsami.1c18330
ACS Appl. Mater. Interfaces 2021, 13, 52736−52742